AIP | The Journal of Chemical Physics

Structure-topology-property correlations of sodium phosphosilicate glasses

Christian Hermansen, Xiaoju Guo, Randall E. Youngman, John C. Mauro, Morten M. Smedskjaer, and Yuanzheng Yue

Citation: The Journal of Chemical Physics **143**, 064510 (2015); doi: 10.1063/1.4928330
View online: http://dx.doi.org/10.1063/1.4928330
View Table of Contents: http://scitation.aip.org/content/aip/journal/jcp/143/6?ver=pdfcov
Published by the AIP Publishing

Structure-topology-property correlations of sodium phosphosilicate glasses

Christian Hermansen,[1] Xiaoju Guo,[2] Randall E. Youngman,[2] John C. Mauro,[2] Morten M. Smedskjaer,[1] and Yuanzheng Yue[1,3,a)]
[1]*Section of Chemistry, Aalborg University, Fredrik Bajers Vej 7H, Aalborg 9220, Denmark*
[2]*Science and Technology Division, Corning Incorporated, Corning, New York 14831, USA*
[3]*State Key Laboratory of Silicate Materials for Architecture, Wuhan University of Technology, Wuhan 430070, China*

(Received 16 January 2015; accepted 29 July 2015; published online 14 August 2015)

In this work, we investigate the correlations among structure, topology, and properties in a series of sodium phosphosilicate glasses with $[SiO_2]/[SiO_2 + P_2O_5]$ ranging from 0 to 1. The network structure is characterized by ^{29}Si and ^{31}P magic-angle spinning nuclear magnetic resonance and Raman spectroscopy. The results show the formation of six-fold coordinated silicon species in phosphorous-rich glasses. Based on the structural data, we propose a formation mechanism of the six-fold coordinated silicon, which is used to develop a quantitative structural model for predicting the speciation of the network forming units as a function of chemical composition. The structural model is then used to establish a temperature-dependent constraint description of phosphosilicate glass topology that enables prediction of glass transition temperature, liquid fragility, and indentation hardness. The topological constraint model provides insight into structural origin of the mixed network former effect in phosphosilicate glasses. © *2015 AIP Publishing LLC.* [http://dx.doi.org/10.1063/1.4928330]

I. INTRODUCTION

Phosphosilicate glasses are known for their complex atomic structure depending on composition, and also for their important technological applications, e.g., as bioactive glasses for regeneration of bone and tissue in the human body. Phosphosilicate glasses consist of a mixture of two prototypical network forming oxides (P_2O_5 and SiO_2), and their composition can be generalized as $xR_2O \cdot (1-x)[ySiO_2 \cdot (1-y)P_2O_5]$, where R_2O is a generic modifying oxide. Phosphosilicate glasses exhibit highly non-linear variation in their physical and chemical properties when one network former is substituted for the other at constant network modifier content. This effect is a general occurrence in mixed network former glasses and is dubbed the mixed network former effect (MNFE).[1–6]

Application of phosphosilicate glasses is mainly focused on silica-rich (high y) compositions. For example, P_2O_5 can be added as a nucleating agent in the production of silicate and aluminosilicate based glass ceramics.[7,8] The original Bioglass® used for regeneration of bone and tissue in the human body is a type of soda lime phosphosilicate glass with $y = 0.95$.[9] Both of these applications rely on the ability of P_2O_5 to react preferentially with the modifying oxide and form pyrophosphate (P^1) or orthophosphate (P^0) units.[10] These P^1 and P^0 units tend to phase separate or crystallize from the glass due to their low connectivity.[11–13] Moreover, these glasses can be transformed to nanocrystal-containing glass-ceramics with special functionality.[14]

From phosphosilicate compositions rich in phosphorous (low y), one can obtain homogeneous glasses.[8,15–20] Such glasses are increasingly used in high technology applications, e.g., as laser component and light emitting materials, if certain types of dopants are introduced and the process conditions are properly controlled.[14,21] However, the structural, dynamical, and thermodynamic properties of phosphate-based glasses have not been well studied partly due to the poor chemical durability that makes the chemical composition and sample characterization inaccurate.[22] Furthermore, these glasses are interesting from a structural point of view, as they exhibit abundant structural and topological features, including six-fold coordinated silicon (Si^6, where the superscript indicates the number of bridging oxygen (BO) in the coordination sphere).[8,17,20,23–25] The formation of Si^6 in phosphosilicate glasses is interesting at ambient pressure because the occurrence of Si^6 is typically limited to high-pressure crystals.[26] Moreover, six-fold coordinated cations are not thought to be network formers in the random network theory of glass structure by Zachariasen.[27]

Phosphosilicate glasses exhibit a large MNFE, but understanding the MNFE in this system has only recently attracted scientific interest.[28,29] At low y, the Si^6 species strongly increase the glass network connectivity, whereas at high y, P_2O_5 preferentially connects with the modifying oxides, leading to a decrease in the phosphate network connectivity, but to an increase in the silicate network connectivity. The low-y compositions containing Si^6 might have especially interesting physical properties such as high hardness and elastic moduli due to the rigid network structure.[28,30] Therefore, it is important to characterize and understand the MNFE in phosphosilicate glasses both from a technological and scientific point of view.

a)Electronic mail: yy@bio.aau.dk

TABLE I. The measured compositions and properties of the $0.3Na_2O \cdot 0.7[y SiO_2 \cdot (1-y)P_2O_5]$ glasses. The compositions of the two glasses with $y = 0.54$ and $y = 0.89$ were not measured, but these were prepared from mixing and re-melting appropriate amounts of $y = 0.43$ and $y = 1$ compositions. In addition to the components given in the table, a small SnO_2 was added to improve fining of the glasses. The largest amount of SnO_2 batched was 0.4 mol. % for the $y = 1$ composition. The experimental details of the measurements are given in the text.

	Analyzed composition (mol. %)			Properties			
y	Na_2O	SiO_2	P_2O_5	T_g (K)	H_V (GPa)	m (...)	ΔC_p ($J \times mol^{-1} \times K^{-1}$)
0	36.4	0	63.6	549	2.0 ± 0.1	37 ± 2	7.9
0.14	31.5	11.3	57.2	630	3.0 ± 0.1	41 ± 2	9.2
0.29	29.3	20.5	50.2	650	3.0 ± 0.1	47 ± 3	10.9
0.43	29.6	29.2	41.2	615	2.7 ± 0.1	38 ± 2	8.8
0.54	...	...	...	581	2.1 ± 0.1	41 ± 1	7.8
0.89	...	...	...	712	3.9 ± 0.1	25 ± 1	4.1
1.00	29.8	70.2	0	739	4.3 ± 0.1	37 ± 1	5.8

In this work, we characterize the structure and physical properties of these glasses and develop a model for describing them. The properties under study include the glass transition temperature (T_g), Vickers indentation hardness (H_V), liquid fragility index (m), and jump in isobaric heat capacity from glass to liquid at the glass transition (ΔC_p), of a series of sodium phosphosilicate glasses with composition $0.3Na_2O \cdot 0.7[y SiO_2 \cdot (1-y)P_2O_5]$. We propose a structural model of Si^6 formation, where a Si^4 unit connects with 2 metaphosphate (P^2) units to create one Si^6 and 2 neutral phosphate (P^3) units. This scheme can quantitatively account for the observation that the Si^6 content is approximately one quarter of the P^3 content. This structural model is used in conjunction with the Gupta-Mauro temperature-dependent constraint theory[31,32] to predict the compositional scaling of physical properties and thus find the origin of the MNFE in phosphosilicate glasses. We note that both the proposed structural and topological constraint models differ from those proposed by Zeng *et al.*[28,29] In detail, their approach does not take into account the role of modifying ions in stabilizing the charge of the Si^6 species, nor the modifying ion sub-network.[33,34] Both aspects are important for explaining the physical properties of phosphosilicate glasses.

II. EXPERIMENTAL

High purity Na_2CO_3, SiO_2, and P_2O_5 powders were batched to prepare a series of $0.3Na_2O \cdot 0.7[y SiO_2 \cdot (1-y)P_2O_5]$ compositions. The mixed powder was melted in platinum crucibles at 1450 °C for 5 h and then roller quenched on a stainless steel plate. The roller quenched cullet was loaded back into the crucible and heated up to 1550 °C for another 15 h. This two-step melting procedure was employed to increase the homogeneity of the glasses, as some of the compositions in the series are hard to become homogeneous during melting.[35,36] Indeed, most of these melts resulted in opaque glasses when they were poured onto a stainless steel plate in air. However, clear glasses could be obtained by roller quenching the melts for compositions containing up to 30 mol. % of SiO_2 ($y = 0.43$). Two additional clear glasses were formed by mixing $y = 0.43$ and $y = 1$ glasses in appropriate amounts, re-melting and roller quenching, thereby yielding glasses with $y = 0.54$ and $y = 0.89$.

The non-crystalline nature of the clear samples was confirmed by X-ray diffraction (XRD), while the opaque silica-rich compositions were found to contain crystalline Na_3PO_4. The chemical compositions of the $0.3Na_2O \cdot 0.7[y SiO_2 \cdot (1-y)P_2O_5]$ glasses were determined by inductively coupled plasma atomic emission spectroscopy (ICP-AES). These analyzed compositions were found to be in good agreement with the batched ones, as seen in Table I. A notable exception was the phosphate-rich sample with $y = 0$, where the analyzed P_2O_5 content is lower than that batched, most likely due to the evaporation of P_2O_5 during melting.

The structure of the glasses was investigated by performing ^{29}Si magic-angle spinning (MAS) nuclear magnetic resonance (NMR) measurements on the $0.3Na_2O \cdot 0.7[y SiO_2 \cdot (1-y)P_2O_5]$ compositions with $y < 0.6$, as well as ^{31}P MAS NMR and Raman spectroscopy measurements on all samples. ^{31}P MAS NMR experiments were conducted at 16.4 T (283.27 MHz resonance frequency) using a commercial spectrometer (VNMRs, Agilent) and 1.6 mm MAS NMR probe. Powdered glasses were packed, using a dry nitrogen-filled glovebag, into 1.6 mm zirconia rotors with sample spinning at 25 kHz. Radio frequency pulses (0.6 μs), corresponding to a $\pi/6$ tip angle, were used along with a 90 s recycle delay to collect 28 acquisitions. The ^{31}P MAS NMR spectra were processed without additional line broadening and frequency (shift) referenced to 85% H_3PO_4 at 0 ppm. The spectra were fit with Gaussian line shapes, using commercial software (Grams), and all spinning sidebands were accounted for in determining the P^n speciation, where n is the number of bridging oxygen bonded to P.

^{29}Si MAS NMR experiments were conducted at 11.7 T (99.28 MHz resonance frequency) using a commercial spectrometer (VNMRs, Agilent) and a 5 mm MAS NMR probe. Glass powders were contained in 5 mm zirconia rotors with sample spinning of 3.3 kHz. 1.3 μs rf pulses ($\pi/6$ tip angle) were used in conjunction with a 180 s recycle delay to collect between 800 and 1400 acquisitions. These ^{29}Si MAS NMR spectra were processed with 100 Hz of additional line broadening, and the chemical shift scale was calibrated against tetramethylsilane at 0.0 ppm. Spectral regions corresponding to silicon with different coordination numbers were integrated to estimate peak areas.

^{23}Na MAS NMR experiments were performed at 16.4 T (185.12 MHz) using a commercial spectrometer (VNMRs, Agilent) and a 1.6 mm MAS NMR probe. Glass samples were typically spun at 25 kHz, and a combination of 0.6 μs rf pulses ($\pi/12$ tip angle) and 1 s recycle delay was used to collect 512 scans. ^{23}Na MAS NMR data were shift referenced to aqueous sodium chloride and processed without any additional apodization.

The following experiments were all performed on glass samples polished to a mirror finish immediately prior to measurement. Raman spectra were collected using a Renishaw inVia Raman microscope in backscatter geometry with a 532 nm solid state laser and then baseline corrected with a second order polynomial expression. The glass transition temperature (T_g) was measured as the onset of the glass transition by differential scanning calorimetry (DSC) at the standard heating rate of 10 K/min[37] (equal to the prior cooling rate). The isobaric heat capacity jump at T_g (ΔC_p) was also determined during the same measurement and it is considered to be a measure of thermodynamic fragility.[5,38,39] ΔC_p was measured by DSC as the difference between the liquid heat capacity (C_{pl}) and the glass heat capacity extrapolated to T_g (C_{pg}). The liquid fragility index (m) could not be determined directly from viscosity-temperature data for the roller-quenched glasses because the samples were too thin. Instead, the values of m were inferred from the activation energy of the glass transition measured by DSC.[40] The activation energy was determined from six DSC cooling/heating rates between 2 and 40 K/min. Indentation hardness was measured on co-planar glass samples with a thickness of approximately 5 mm (or 1 mm for roller-quenched glasses) using a Vickers diamond with a load of 490 mN and a 15 s press time. The reported hardness value represents an average over 25 well separated indents.

III. STRUCTURE

The silicate network structure of phosphosilicate glasses at low y is dominated by the formation of the Si^6 network forming unit (NFU).[8,41] In general, the formation of Si^6 in phosphosilicate glasses can be understood by the concept of optical basicity.[42] Optical basicity is a measure of the effective negative charge on oxygen, and it is determined by the UV absorbance wavelength of probe ions such as Tl^+, Pb^{2+}, or Bi^{3+}.[42] The optical basicity of SiO_2 is higher than that of P_2O_5, so the effective negative charge on the oxygen in SiO_2 is also higher than that in P_2O_5.[43] When a small amount of SiO_2 is added to P_2O_5, the positive charge on Si^{4+} must be balanced by oxygen with relatively low effective negative charge. Because more oxygen ions than the usual four are required to balance the positive charge on silicon, then silicon can assume a coordination number of six instead of the usual four in SiO_2.

Yamashita *et al.*[43] have investigated the correlation between optical basicity and the fraction of Si^6 in alkali phosphosilicate glasses and found that optical basicity alone cannot quantitatively predict the fraction of Si^6. A quantitative relation between the Si^6 concentration and the P^3 concentration was observed by Jiang *et al.*[29] They found that the Si^6 concentration is approximately equal to one fourth of the expected P^3 concentration in a variety of phosphosilicate glasses. This result can be understood by the microscopic Si^6 formation mechanism suggested by Miyabe *et al.*,[41] who found that a Si^4 NFU bound to four P NFUs can connect with two P^2 NFUs to create a Si^6 with six P NFU neighbors. The two P^2 NFUs are converted to P^3 in this reaction, and the modifying cations that are charge balancing P^2 will instead charge balance the $[SiO_{6/2}]^{2-}$ (Si^6) NFU. Thus, Si^6 requires charge balancing by the modifying ions much like four-fold coordinated boron in borate and borophosphate glasses.[32,44] The occurrence of Si^6 in modifier-free phosphosilicate glasses has also been reported,[24,25] and this cannot be explained by the formation mechanism suggested by Miyabe *et al.*[41] Modifier-free phosphosilicate glasses can easily be partially crystallized to SiP_2O_7,[24] which contains six-fold coordinated silicon, indicating that the formation of Si^6 in these glasses is related to nucleation of a SiP_2O_7 crystalline phase.[25] The formation mechanism of Si^6 in sodium phosphosilicate glasses based on the work of Miyabe *et al.*[41] and Jiang *et al.*[29] is shown in Fig. 1.

Fig. 1 shows a Si^4 NFU having four P^3 NFU neighbors connecting with two P^2. The product is a Si^6 NFU with six P^3 NFU neighbors and charge balanced by two Na^+ ions. The P^3 NFUs stabilize Si^6, possibly by charge-delocalization, and can therefore only have a single Si^6 NFU neighbor. This is why the Si^6 concentration is approximately one-sixth of the actual P^3 concentration or one-fourth of the expected P^3 concentration if Si^6 is not charge compensated.

In summary, the formation of Si^6 is thus limited by the modifying oxide, silica, and P^3 concentrations. The Si^6 concentration in homogenous sodium phosphosilicate glasses

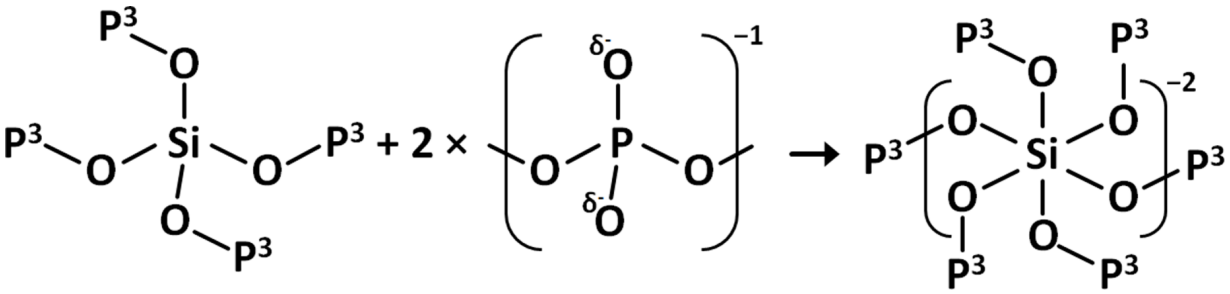

FIG. 1. The mechanism of Si^6 formation in phosphosilicate glasses is proposed to be as follows: a Si^4 NFU with four P^3 NFU neighbors connects with two P^2 NFU to form a Si^6 NFU with six P^3 NFU neighbors. In the process, the two P^2 are converted to P^3, and the negative charge and charge stabilizing modifying ions are transferred to the Si^6 NFU. P^3 is a neutral phosphate unit with three bridging oxygen and one double bonded terminal oxygen.

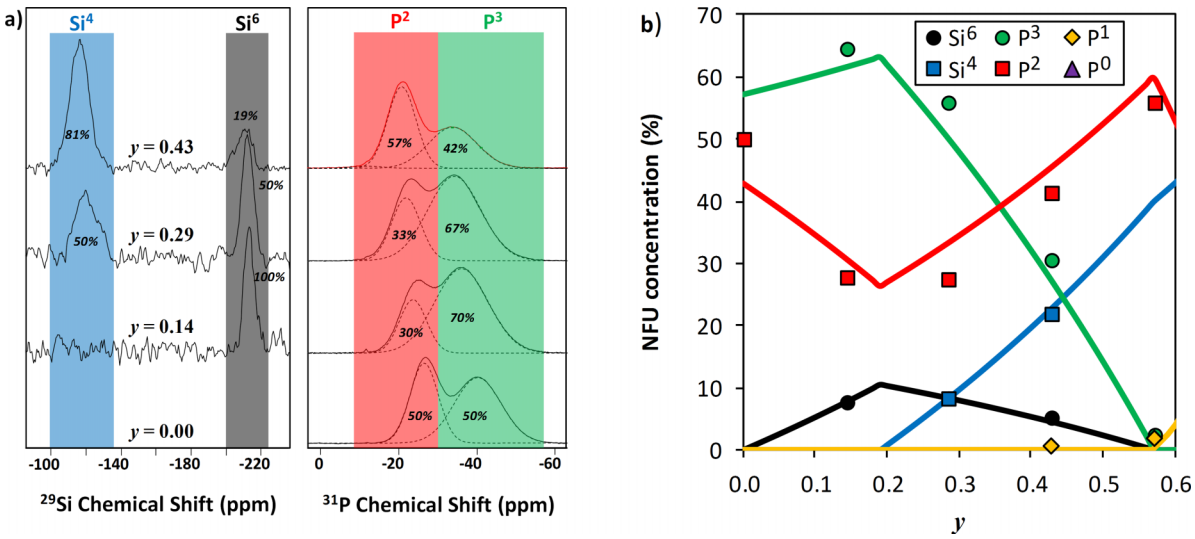

FIG. 2. (a) ^{29}Si and ^{31}P MAS NMR spectra of the $0.3Na_2O \cdot 0.7[ySiO_2 \cdot (1-y)P_2O_5]$ glasses with $y \leq 0.43$. The chemical shift ranges belonging to each NFU are highlighted, and the area ratios obtained by deconvoluting the spectra are indicated. The NFUs are named based on the Q^n terminology, where Q is the network forming cation, and n is the number of bridging oxygen in the coordination sphere. (b) The network forming unit (NFU) fractions derived from the ^{29}Si and ^{31}P MAS NMR spectra and the compositions of the $0.3Na_2O \cdot 0.7[ySiO_2 \cdot (1-y)P_2O_5]$ glasses. The solid lines represent the structural model from Section III.

with the generalized composition $xNa_2O \cdot (1-x)[ySiO_2 \cdot (1-y)P_2O_5]$ can be quantified as

$$Si^6(x,y) = \min\left[x, (1-x)\,y, \frac{(1-x)(1-y)-x}{2}\right]. \quad (1)$$

Using Eq. (1) and the well-established knowledge about the chemistry of phosphate and silicate glasses, we propose a predictive structural model for phosphosilicate glasses. Based on the work of Miyabe *et al.*,[41] Si^6 is taken to be the preferred charge-balancing species in these glasses, and other reactions will only occur when a higher concentration of modifying oxide that can be charge balanced by Si^6 is present. Further modification occurs in the phosphate network, and the P NFU concentrations are determined by Van Wazer's depolymerization model.[22,45] When the phosphate network is fully depolymerized to P^0, the silicate network begins to become modified. The silicate network is also sequentially depolymerized from Si^4 to Si^0 (orthosilicate). As shown in Fig. 2, this structural model agrees well with the experimentally determined NFU fractions from the deconvoluted ^{29}Si and ^{31}P MAS NMR spectra of the $0.3Na_2O \cdot 0.7[ySiO_2 \cdot (1-y)P_2O_5]$ glasses.

Prior to deconvoluting the ^{29}Si and ^{31}P MAS NMR spectra, the sodium environment was probed by ^{23}Na MAS NMR in order to evaluate the glass homogeneity beyond the resolution of the XRD. The ^{23}Na MAS NMR spectra are seen in Fig. 3 alongside ^{31}P MAS NMR spectra of the three phosphosilicate compositions with highest silica contents. Broad and symmetric ^{23}Na Gaussian line shapes were obtained for all compositions, except for two compositions with $y = 0.54$ and $y = 0.89$. These two compositions show distorted ^{23}Na MAS NMR peak shapes, and this is a reflection of inhomogeneity in the sodium coordination environment. The ^{31}P MAS NMR spectra of the $y = 0.54$ and $y = 0.89$ compositions contain numerous new resonances compared to $y = 0.43$, which we believe is homogenous. This clearly indicates crystallization, most likely of sodium orthophosphate (P^0) and sodium pyrophosphate (P^1), although the broad peaks indicate that the crystals are small and possibly disordered. Despite lack of perfect homogeneity in the $y = 0.54$ and $y = 0.89$ compositions, we have chosen to include their structural and physical data in order to give a broad picture about the structure of the phosphosilicate system.

Raman spectroscopy was performed to support the structural characterization by ^{29}Si and ^{31}P MAS NMR spectroscopy. The structural model in Fig. 2 is also supported by the Raman spectra of the $0.3Na_2O \cdot 0.7[ySiO_2 \cdot (1-y)P_2O_5]$ glasses shown in Fig. 4. The Raman spectrum of the $y = 0$ composition contains three main peaks, which are assigned to

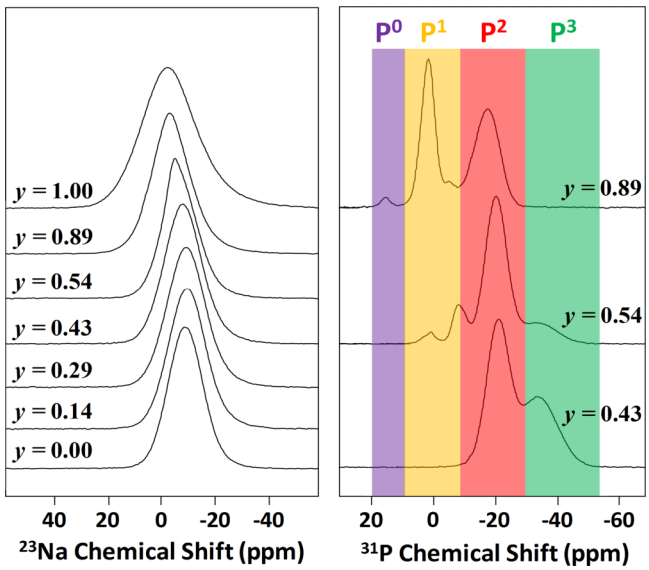

FIG. 3. ^{23}Na and ^{31}P MAS NMR spectra of the $0.3Na_2O \cdot 0.7[ySiO_2 \cdot (1-y)P_2O_5]$ glasses (^{31}P MAS NMR spectra only for compositions with $0.4 < y$). The chemical shift ranges belonging to each P NFU are highlighted.

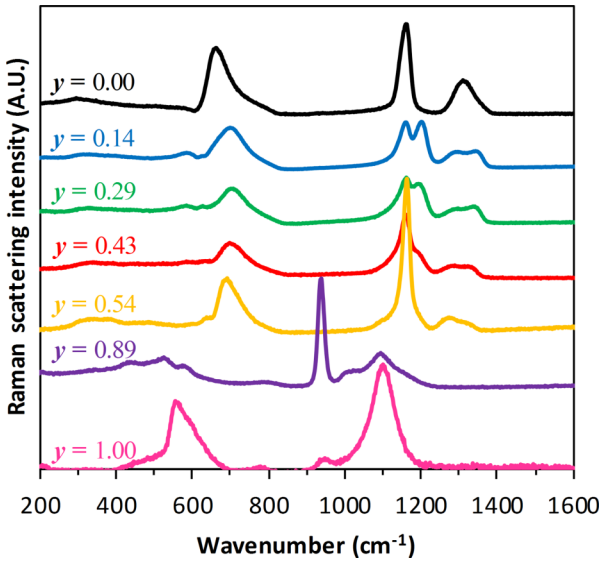

FIG. 4. Raman spectra of $0.3Na_2O \cdot 0.7[ySiO_2 \cdot (1-y)P_2O_5]$ glasses normalized by total scattering intensity. The Raman cross section of P NFUs is much larger than for Si NFUs, and features of Si NFUs cannot be discerned in compositions with $0 \le y \le 0.54$. The band assignment is discussed in the text.

the symmetrical stretching modes of P═O (P^3) at 1310 cm^{-1}, PO_2^- (P^2) at 1160 cm^{-1}, and P–O–P at 667 cm^{-1}, respectively.[46] With increasing silica content, several changes occur in the Raman spectra, most importantly a peak appears at 1200 cm^{-1}, which has previously been observed in Si^6-containing phosphosilicate glasses.[43] We assign this peak to the symmetrical P═O stretching of a P^3 unit with a Si^6 next-nearest neighbor. This assignment is based on the correlation between peak intensity and Si^6 and P^3 concentrations as determined from the ^{29}Si and ^{31}P MAS NMR data in Fig. 2. In addition, the band originally centered at 1310 cm^{-1} is split into two at about 1340 cm^{-1} and 1290 cm^{-1}. A similar splitting of this band has been observed for modifier-free phosphosilicate glasses, which was attributed to the change of P═O (P^3) vibrational frequency with P^3 having Si next-nearest neighbors.[19] The vibrational frequency increases with a decreasing electron density in the P═O bond,[19] and as Si is less electronegative than P, the low frequency component is expected to correspond to P^3 with Si NFU neighbors. The compositional trends of peak intensities appear to confirm this expectation, as the 1290 cm^{-1} peak intensity increases with y, while the 1340 cm^{-1} peak intensity decreases. It should be noted that the alkali oxide content in alkali phosphate glass also influences the vibrational frequency of the P═O bond, where more alkali oxide leads to a lower wavenumber.[46] However, this effect has not been observed to cause a splitting of the band, as occurs in phosphosilicate glasses.[19]

The P–O–P band at 667 cm^{-1} found in the $y = 0$ composition is shifted to about 700 cm^{-1} upon silica addition ($y = 0.14$), and then, the peak position remains almost unchanged. In sodium phosphate glasses, the frequency of this band increases with the Na_2O content, and a frequency of 700 cm^{-1} is reached for the metaphosphate ($x = 0.5$) composition.[46] The blue-shift in phosphosilicate glasses could be due to both the depolymerization of the phosphate network and the formation of P^3–O–Si bonds with a Raman shift around 710 cm^{-1}.[19]

For the $y = 0.54$ composition, a sharp peak assigned to the symmetrical stretching of PO_2^- (P^2) dominates the spectrum, which agrees with the ^{31}P MAS NMR spectrum in Fig. 3 showing that the phosphorous speciation is dominated almost exclusively by P^2. The sharpness of the PO_2^- (P^2) peak further supports that this composition is partially crystalline, although it is XRD amorphous. The same is the case for the $y = 0.89$ composition which is also XRD amorphous but has a dominant sharp peak at 940 cm^{-1} due to asymmetrical stretching of PO_2^{3-} (P^0). This is probably due to a small fraction of Na_3PO_4 crystals,[14,47] as also inferred from the ^{23}Na and ^{31}P MAS NMR results. A signature of P^1 units is found at 1000 cm^{-1}, which is the frequency of asymmetrical stretching of PO_2^{2-} (P^1).[47] In this composition, it is also possible to see low intensity features of the silicate network. The peak at 1100 cm^{-1} is caused by the symmetrical stretching of SiO_2^- (Si^3), and the shoulder at about 1150 cm^{-1} is due to SiO_2 (Si^4).[47,48] The bands in the range of 430–600 cm^{-1} are attributed to the symmetrical stretching of Si–O–Si with different numbers of bonding oxygen of the Si NFUs.[48] The Raman spectrum of the $y = 1$ composition almost exclusively shows Si^3 units and Si–O–Si bonding.

IV. TOPOLOGY

Topological constraint theory as applied to glasses was introduced in a series of seminal papers by Phillips and Thorpe[49–57] and extended by Gupta and Mauro[31,32] to give a temperature dependent form that can quantitatively predict glass properties such as T_g, fragility, and indentation hardness.[6,31,32,58] It has been successfully applied to explain the MNFE in borosilicate,[6] boroaluminosilicate,[59] and borophosphate[44] glasses. The theory links the short-range structures of the network formers[32] and network modifiers[33,34] to a number of constraints that hinder the free movement of atoms. Any effects due to intermediate-range or long-range order are usually not taken into account, and the glass is therefore assumed to be perfectly homogeneous. Generally, only two types of constraints are considered: linear bond stretching constraints corresponding to chemical bonds and angular bond bending constraints corresponding to bond angles. The number of linear and angular constraints around a network forming atom can be calculated as[55]

$$n_{c,linear} = \frac{1}{2}\mathrm{CN}\Big|_{\mathrm{CN}\ge 2}, \tag{2}$$

$$n_{c,angular} = (2\mathrm{CN} - 3)|_{\mathrm{CN}\ge 2}, \tag{3}$$

where CN is the coordination number of the atom in question. In oxide glasses, the network formers are exclusively coordinated by oxygen, and it is convenient to attribute all the linear constraints in a NFU to the oxygen atoms. There are two linear constraints per BO and one linear constraint per non-bridging oxygen (NBO) when counting in this manner, corresponding to the Si–O or P–O bonds. The angular constraints are counted on O, Si, or P, and are calculated by Eq. (3).

The procedure used to account for the constraints related to the modifying cations is debatable and not as straightforward as for the network forming cations. The modifying cations

form ionic bonds to NBOs and have high CN, but in spite of their high CN, modifying cations break up the network and lower the average number of constraints per atom. We have previously introduced the concept of a modifying ion sub-network to explain the effect of modifying ions on glass properties using temperature-dependent constraint theory.[33] In this approach, we assume that Eq. (3) is invalid for ionic bonding, as this type of bonding is non-directional.[33] Furthermore, because the individual ionic bonds are rather weak, they can easily be thermally activated, and a significant fraction of the linear constraints by Eq. (2) may not be intact.[34] This can be taken into account by utilizing the concept of constraint strength.[34,60]

We derive a topological model of sodium phosphosilicate glass by applying Eqs. (2) and (3) to the NFUs and by considering the modifying ion sub-network constraints. Thus, we consider the following constraints:

- α: Si–O and P–O linear constraints. There are two at each BO and one at each NBO. None are counted at the double bonded terminal oxygen (TO) on P^3 as it is not considered to be a part of the network.[34]
- β: O–Si–O and O–P–O angular constraints. There are nine for Si^6, five for Si^4, Si^3, Si^2, Si^1, Si^0, P^2, P^1, and P^0, respectively, but only three for P^3. P^3 is considered to be effectively three-fold coordinated because the TO is not part of the network.
- γ: Na^+–NBO linear constraints. The number of constraints is equal to the oxygen CN of Na^+ charge balancing NBO. There are no constraints for Na^+ charge balancing Si^6.
- δ: Si–O–Si, Si–O–P, and P–O–P angular constraints. There is one for each BO. No angular constraints are counted for NBO.

The analytical expressions for the number of constraints (n_c) in phosphosilicate glasses with composition $x\mathrm{Na_2O} \cdot (1-x)[y\mathrm{SiO_2} \cdot (1-y)\mathrm{P_2O_5}]$ are derived from the speciation of the NFUs as described in Section III and given as

$$n_{c,\alpha}(x,y) = 2 \times \mathrm{BO}(x,y) + 1 \times \mathrm{NBO}(x,y), \tag{4a}$$

$$\begin{aligned} n_{c,\beta}(x,y) = {} & 9 \times \mathrm{Si^6}(x,y) + 3 \times \mathrm{P^3}(x,y) \\ & + 5 \times \left[\mathrm{P^2}(x,y) + \mathrm{P^1}(x,y) + \mathrm{P^0}(x,y)\right] \\ & + 5 \times \left[\mathrm{Si^4}(x,y) + \mathrm{Si^3}(x,y)\right. \\ & \left. + \mathrm{Si^2}(x,y) + \mathrm{Si^1}(x,y) + \mathrm{Si^0}(x,y)\right], \end{aligned} \tag{4b}$$

$$n_{c,\gamma}(x,y) = \mathrm{CN} \times \mathrm{Na^+_{NBO}}(x,y), \tag{4c}$$

$$n_{c,\delta}(x,y) = 1 \times \mathrm{BO}(x,y). \tag{4d}$$

For convenience, we consider the Si—O and P—O linear constraints equivalent and denote them as the strongest (α) constraint. The second strongest (β) constraint is the O–Si–O and O–P–O angular constraints. The Na^+—NBO linear γ constraint in sodium phosphate glasses is found to be only partially intact at T_g,[34] and we denote this as the third strongest constraint. The BO centered angular δ constraint is generally considered broken at T_g, even for low T_g compositions such as B_2O_3, and we consider this to be the weakest constraint.[6,32,33,44]

V. GLASS TRANSITION TEMPERATURE

The glass transition temperature is determined as the onset temperature of the glass transition by DSC at a heating rate equal to the prior cooling of 10 K/min. The DSC scans of the $0.3\mathrm{Na_2O} \cdot 0.7[y\mathrm{SiO_2} \cdot (1-y)\mathrm{P_2O_5}]$ glasses are shown in Fig. 5. T_g is determined as the intercept of the extrapolated glass C_p and the inflection of the curve. The T_g values of the $0.36\mathrm{Na_2O} \cdot 0.64\mathrm{P_2O_5}$ ($y = 0$) and $0.30\mathrm{Na_2O} \cdot 0.70\mathrm{SiO_2}$ ($y = 1$) end-member compositions are close to those reported in the literature for anhydrous glasses.[33,34,61] The T_g is plotted vs. y in Fig. 6 and exhibits a MNFE as a sharp local maximum around the $y = 0.29$ composition and a local minimum apparently around $y = 0.54$, which is at the edge of the glass-forming region. The trend of the MNFE in T_g closely matches the fraction of Si^6 from the structural model in Fig. 2(b) and can be accounted for by temperature dependent constraint theory.[6,31,32,44]

The Adam-Gibbs theory which links viscosity to configurational entropy[62,63] is used as the physical basis relating T_g to the number of network constraints. Naumis has derived the configurational entropy function from the number of floppy modes,[64] i.e., the atomic degrees of freedom. By considering T_g as the isokom temperature at which the viscosity is equal to 10^{12} Pa s[37,65] and assuming that the potential energy barrier to viscous flow is unchanged with composition, then an equation can be derived which relates the T_g ratios of two compositions to the inverse ratio of the corresponding degrees of freedom. A detailed derivation and description can be found elsewhere,[31,32] and the result is

$$\frac{T_g(x,y)}{T_{g,ref}} = \frac{f\left[T_{g,ref}, x_{ref}, y_{ref}\right]}{f\left[T_g(x,y), x, y\right]} = \frac{3 - N_c\left[T_{g,ref}, x_{ref}, y_{ref}\right]}{3 - N_c\left[T_g(x,y), x, y\right]}, \tag{5}$$

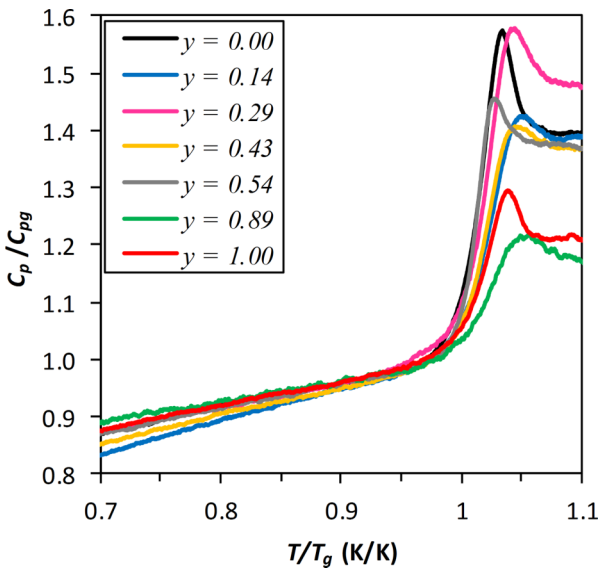

FIG. 5. Differential scanning calorimetry scans for the $0.3\mathrm{Na_2O} \cdot 0.7[y\mathrm{SiO_2} \cdot (1-y)\mathrm{P_2O_5}]$ glass compositions. C_p is given per mole of atoms in the glass.

where f is the number of degrees of freedom and N_c is the number of rigid constraints at T_g per network forming atom. Equation (5) requires that $0 < f[T_g, x, y] < 3$.

For sodium phosphosilicate glasses with composition $x\mathrm{Na_2O} - (1-x)[y\mathrm{SiO_2} - (1-y)\mathrm{P_2O_5}]$, $N_c[T_g(x,y), x, y]$ is determined by the number of intact constraints in Eqs. (4a)–(4d). Thus, the average number of constraints per atom at T_g is

$$N_c(x,y,T_g) = 2 \times \mathrm{BO}(x,y) + 1 \times \mathrm{NBO}(x,y) + 9 \times \mathrm{Si}^6(x,y) + 3 \times \mathrm{P}^3(x,y) + 5 \times \left[\mathrm{P}^2(x,y) + \mathrm{P}^1(x,y) + \mathrm{P}^0(x,y)\right] + 5 \times \left[\mathrm{Si}^4(x,y) + \mathrm{Si}^3(x,y) + \mathrm{Si}^2(x,y) + \mathrm{Si}^1(x,y) + \mathrm{Si}^0(x,y)\right] + q_\gamma(T_g) \times \mathrm{CN_{Na}} \times \mathrm{Na^+_{NBO}}(x,y). \quad (6)$$

Here, $q_\gamma(T_g)$ represents the constraint strength[34,60] for the γ constraint at T_g and is used to reflect that the γ constraints are not fully intact. In isostructural metaphosphate glasses, the constraint strength depends on the charge and size of the modifying cation.[34,60] Although the structure of the glass changes from a phosphate-based network at $y = 0$ to a silicate network at $y = 1$, we have approximated the constraint strength as a constant $q_{\gamma,\mathrm{Na}}(T_g) = 0.4$ with $\mathrm{CN_{Na}} = 5$.[34] This corresponds to 2 γ constraints per $\mathrm{Na^+}$, which is in good agreement with our previous work on alkali phosphate glasses[33,34] and the results of a recent molecular dynamics simulation of soda lime silicate glasses.[66] The BO centered angular δ constraint is considered broken at T_g.[6,32,33,44]

The structural model outlined in Section III is used to evaluate the concentrations of each network forming atom. We can then predict the composition dependence of T_g by introducing Eq. (6) into Eq. (5) and using the pure $\mathrm{P_2O_5}$ glass as reference with $T_{g,ref} = 590$ K[67] and $N_c(T_{g,ref}, x_{ref}, y_{ref}) = 2.4$.[33] The modeled composition dependence of T_g is plotted in Fig. 6 together with experimental values determined by DSC. The model and experiment differ up to ±50 K for the $0.3\mathrm{Na_2O} \cdot 0.7[y\mathrm{SiO_2} \cdot (1-y)\mathrm{P_2O_5}]$ glass series, but the observed compositional trend is well reproduced by the model without any adjustable fitting parameters. In the derivation of Eq. (5) from the Adam-Gibbs equation, it was assumed that the potential energy barrier to viscous flow does not change with composition. This is a reasonable approximation within a family of glasses, e.g., silicate systems, but may be problematic in a mixed-network former glass. This may be the cause of the model overestimating T_g in the middle y region, but underestimating in the high-y region.

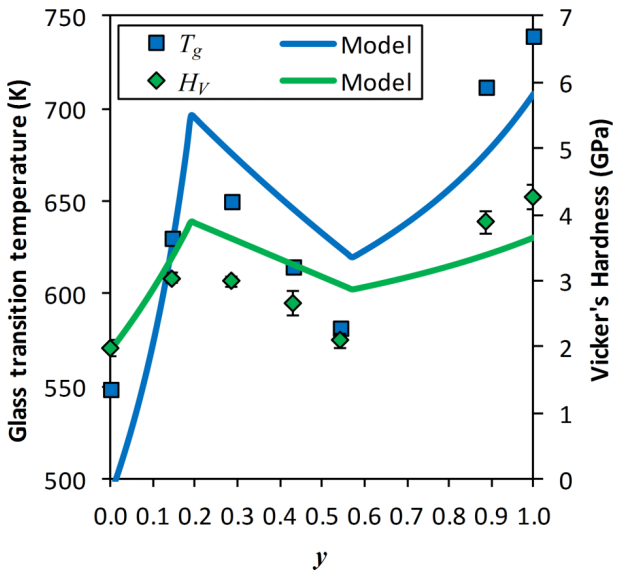

FIG. 6. Compositional dependence of the glass transition temperature and indentation hardness for the $0.3\mathrm{Na_2O} \cdot 0.7[y\mathrm{SiO_2} \cdot (1-y)\mathrm{P_2O_5}]$ glass compositions. The squares represent experimental T_g determined by DSC, and the diamonds represent experimental H_V by Vickers microindentation. The solid lines represent the modeled properties by Eqs. (5) and (11).

We also performed a separate study on soda-lime-phosphosilicate glasses with composition $0.1\mathrm{CaO} \cdot 0.2\mathrm{Na_2O} \cdot 0.7[y\mathrm{SiO_2} \cdot (1-y)\mathrm{P_2O_5}]$. The aim of this separate study was to see if the results obtained here could readily be used to model a more complex system. However, in the soda-lime-phosphosilicate system, a single constraint strength as given in Eq. (6) does not appear to be sufficient to describe the experimental data.

VI. FRAGILITY

The liquid fragility (m) of the glasses was determined indirectly by DSC measurements from the change in fictive temperature (T_f) with cooling rate (Q),[40]

$$\log\left(\frac{Q}{Q_{ref}}\right) = m - m \times \frac{T_{f,ref}}{T_f}, \quad (7)$$

where Q is heating and previous cooling rate through the glass transition region, Q_{ref} is the reference heating and cooling rate taken as 10 K/min, and $T_{f,ref}$ is the fictive temperature corresponding to Q_{ref} and equivalent to our calorimetric definition of T_g.

In order to confirm the liquid fragility results obtained by DSC, the m of the $0.3\mathrm{Na_2O} \cdot 0.7\mathrm{SiO_2}$ ($y = 0$) composition was also determined from direct measurements of the temperature dependence of viscosity. The viscosity was measured with a rotational viscometer at low viscosities (approximately 10^0-10^2 Pa s) and ball penetration viscometer at high viscosities (10^{10}-10^{12} Pa s). The viscosity data were fitted to the Mauro-Yue-Ellison-Gupta-Allan (MYEGA) equation[68] and m was equivalent within the standard deviation to that determined by DSC with Eq. (7).

The m values of the $0.3\mathrm{Na_2O} \cdot 0.7[y\mathrm{SiO_2} \cdot (1-y)\mathrm{P_2O_5}]$ glasses are plotted as a function of y in Fig. 7. In this figure, the isobaric heat capacity jump at T_g (ΔC_p) is also plotted against y and has a very similar trend as the m data. It is also seen that at $y = 0.89$, the fragility is lower than the general compositional trend. This can be ascribed to the fact that the $\mathrm{P^0}$ units detected by ^{23}Na, ^{31}P MAS NMR, and Raman spectroscopy do not participate in the glass network due to phase separation or crystallization, while the model assumes the glass

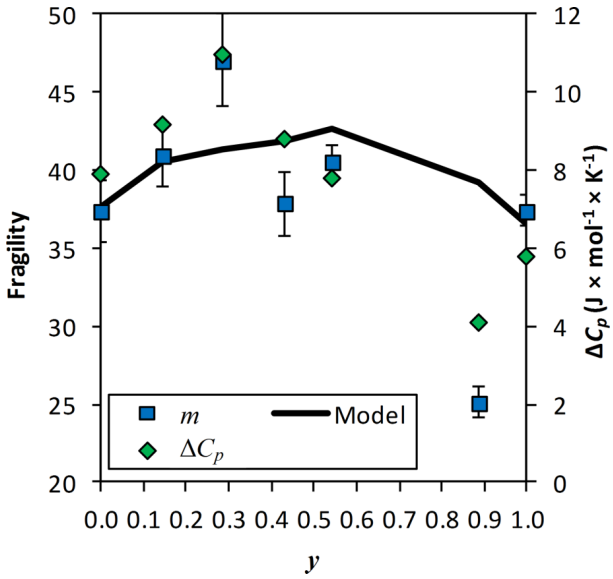

FIG. 7. Compositional dependence of the liquid fragility (m) and thermodynamic fragility (ΔC_p) for the $0.3Na_2O \cdot 0.7[ySiO_2 \cdot (1-y)P_2O_5]$ glass compositions. The squares represent experimental m determined by DSC, and the diamonds represent experimental ΔC_p (equal to $C_{pl} - C_{pg}$). The solid lines represent the modeled properties by Eqs. (8)–(10).

to be perfectly homogeneous. The fragility peaks at $y = 0.29$, where both the T_g and the Si^6 content are also the highest.

The relation between liquid fragility and the network constraints was first found by Gupta and Mauro.[31,32] They suggested that the liquid fragility is related to the change in degrees of freedom per atom at T_g and quantified it using

$$m(x,y) = m_0 \left(1 + \frac{\partial \ln f(x,y,T)}{\partial \ln T}\right)\Bigg|_{T=T_g(x)}, \quad (8)$$

where m_0 is the fragility index of an ideally strong liquid taken to be 15.[31] In order to take the temperature derivative of $\ln f(x,y,T)$, a continuous function is needed. The fraction of rigid constraints is estimated to depend on temperature as

$$q_i(T) = \left[1 - \exp\left(-\frac{\Delta F_i^*}{k_B T}\right)\right]^{vt_{obs}}, \quad (9)$$

where ΔF_i^* is the activation energy for breaking constraint i and vt_{obs} is the product of the vibrational attempt frequency and observation time.[31] The activation energy is related to a characteristic constraint onset temperature by

$$\Delta F_i^* = -k_B T_i \ln\left(1 - 2^{-1/vt_{obs}}\right), \quad (10)$$

where T_i is the constraint onset temperature of constraint i and can be considered to be the temperature at which the constraint goes from intact to broken.[32]

We model m by combining Eqs. (8)–(10) with the topological model in Section IV. This approach requires the constraint onset temperatures and vt_{obs}, but these parameters cannot be measured directly. In our previous work on the topology of borosilicate glasses, we found that $vt_{obs} = 60$ and the oxygen bond stretching α constraint onset temperature $T_\alpha = 1600$ K and $T_{\beta,Si} = 1425$ K.[6] As a first approximation, we use the same values for phosphosilicate glasses, although there are some indications that Si^6 has a lower $T_{\beta,Si}$. The onset temperature of the bond bending β constraint around P ($T_{\beta,P}$) is taken from our analysis of the topology of alkali phosphate glasses where $T_{\beta,P} = 850$ K.[33] The onset temperature of the oxygen centered bond bending δ constraint (T_δ) is inferred from the Vogel temperature of B_2O_3 to be 328 K[32] and was also used in our work on alkali phosphate glasses.[33] This leaves only the onset temperature of the modifying ion bond stretching γ constraint as a fitting parameter. By fitting to the experimental m values, the onset temperature $T_{\gamma,Na} = 600$ K is obtained, which agrees well with that obtained previously on sodium phosphate glasses.[33]

The compositional dependence of m modeled by Eqs. (8)–(10) is plotted in Fig. 7 together with the experimental m and ΔC_p values determined by DSC. The maximum in the experimental m and ΔC_p at $y = 0.29$ is not replicated by the model. It is known that the amount of Si^6 in phosphosilicate glasses depends not only on composition but also on the cooling rate.[8] A higher cooling rate can trap a higher amount of Si^6 in glass. This means that the Si—O bonds of Si^6 units are dynamically forming and breaking during quenching, and the remaining amount of Si^6 depends on the cooling rate, much like the cooling rate dependence of the boron speciation in borate glasses.[69] The Si^6-containing glass compositions with a stronger cooling rate dependence of silicon speciation are more fragile than those with a weaker cooling rate dependence. The increase in fragility can be modeled by lowering the constraint onset temperatures of the Si^6 NFUs. However, for simplicity, we have taken T_α and $T_{\beta,Si}$ to be the same for all Si NFUs in Fig. 7. The model reproduces the compositional scaling of m and ΔC_p with reasonable accuracy except for the glasses containing a large amount of Si^6 and for the inhomogeneous glass with $y = 0.89$.

VII. INDENTATION HARDNESS

The Vickers indentation hardness (H_V) is plotted as a function of y together with the T_g values in Fig. 6. The compositional trends of H_V and T_g are very similar, and they both exhibit a maximum around $y = 0.2$, i.e., around the maximum fraction of Si^6 in our structural model.

A relation between the indentation hardness and the network constraints was first proposed by Smedskjaer *et al.*[58] and has since been used to predict the compositional dependence of hardness in borate,[58] borosilicate,[6] boroaluminosilicate,[59] and borophosphate[44] glass compositions. The relation is

$$H_V(x,y) = \left(\frac{dH_V}{dN_c}\right) \times (N_c(x,y,T = 298\text{ K}) - N_{c,crit}). \quad (11)$$

Here, $N_c(x,y,T = 298$ K) is the number of constraints per network forming atom at room temperature for composition (x, y), dH_V/dN_c is the load-dependent proportionality on the order of 10 GPa,[58] and $N_{c,crit}$ is the minimum number of constraints per atom necessary to significantly affect the hardness and was found to be approximately 2.5 (corresponding to rigidity in two dimensions).[58]

The intact constraints at room temperature can be enumerated by using the topological model in Section IV,

$$N_c(x,y,T=298\text{ K}) = 3\times \text{BO}(x,y) + 1\times \text{NBO}(x,y) + 9\times \text{Si}^6(x,y) + 3\times \text{P}^3(x,y) + 5\times\left[\text{P}^2(x,y)+\text{P}^1(x,y)+\text{P}^0(x,y)\right] + 5\times\left[\text{Si}^4(x,y)+\text{Si}^3(x,y)+\text{Si}^2(x,y)+\text{Si}^1(x,y)+\text{Si}^0(x,y)\right] + q_\gamma(T=298\text{ K})\times \text{CN}_{\text{Na}}\times \text{Na}^+_{\text{NBO}}(x,y)\,. \quad (12)$$

The difference between Eqs. (12) and (6) is the following. In Eq. (12), the δ BO angular constraint is considered to be intact, and the γ constraints have increased rigidity due to $q_\gamma(T_g) < q_\gamma(T = 298\text{ K})$. We find $q_{\gamma,\text{Na}}(T = 298\text{ K})$ to be 0.6, yielding 3 γ constraints per Na^+ at room temperature.

The modeled composition dependence of H_V described by Eq. (11) with $(dH_V/dN_c) = 7.5$ GPa and $N_{c,crit} = 2.5$ is plotted in Fig. 6 and compared to experimental values determined by Vickers microindentation. The model manages to capture the composition trend of the indentation hardness, but the difference between the modeled and experimental values is up to ±1 GPa for the $0.3Na_2O \cdot 0.7[y SiO_2 \cdot (1-y) P_2O_5]$ glass series. Our model for phosphosilicate glass utilizes the same approach and parameters that have been successfully applied to describe the compositional dependence of hardness of borate,[58] borosilicate,[6] boroaluminosilicate,[59] and borophosphate[44] glass compositions. For this reason, the rather large difference between the absolute values of model and experiment is surprising and still needs to be further investigated. Zeng *et al.*[28] achieved a higher fidelity between model and experiment by taking $N_{c,crit}$ to increase with the degree of polymerization of the glass network. However, we do not find it reasonable to take $N_{c,crit}$ to be a free variable, partly because it has been found to be a constant for a wide range of glasses,[6,44,58,59] but also because a large $N_{c,crit}$ completely fails to account for the *high* hardness of the silicate-rich compositions.

VIII. CONCLUSION

By combining structural and topological modeling with experimental results, we have provided new insights into the structure-topology-property relations of sodium phosphosilicate glasses. The topological modeling approach is based on temperature-dependent constraint theory, which relies on accurate knowledge of the composition dependence of NFU speciation. We have therefore proposed a structural model of the NFU concentrations in these glasses, which is based on the formation mechanism of the six-fold coordinated Si (Si^6).[41] An important aspect of the Si^6 formation mechanism is that the modifying sodium ions charge-stabilize Si^6, but cannot simultaneously modify the phosphate network. From this structural model, we have performed a topological analysis of the glass system by associating temperature-dependent constraints with various NFUs. This model captures the overall composition-property relation and MNFE of the glass transition temperature, indentation hardness, and fragility. Our approach also provides insight into the glass transition phenomenon in network glasses.

[1] D. Larink, H. Eckert, M. Reichert, and S. W. Martin, J. Phys. Chem. C **116**, 26162 (2012).
[2] M. T. Rinke and H. Eckert, Phys. Chem. Chem. Phys. **13**, 6552 (2011).
[3] R. B. Christensen, *The Mixed Glass Former Effect in* $0.35Na_2O + 0.65[xB_2O_3 + (1-x)P_2O_5]$ *Glasses* (Iowa State University, 2012).
[4] C. M. Bischoff, *The Mixed Glass Former Effect in* $0.5Na_2S + 0.5[xGeS_2 + (1-x)PS_{5/2}]$ *Glasses* (Iowa State University, 2013).
[5] Q. Zheng, M. Potuzak, J. C. Mauro, M. M. Smedskjaer, R. E. Youngman, and Y.-Z. Yue, J. Non-Cryst. Solids **358**, 993 (2012).
[6] M. M. Smedskjaer, J. C. Mauro, R. E. Youngman, C. L. Hogue, M. Potuzak, and Y.-Z. Yue, J. Phys. Chem. B **115**, 12930 (2011).
[7] A. K. Varshneya, *Fundamentals of Inorganic Glasses* (Gulf Professional Publishing, 1994), pp. 83–84.
[8] R. Dupree, D. Holland, M. G. Mortuza, J. A. Collins, and M. W. G. Lockyer, J. Non-Cryst. Solids **106**, 403 (1988).
[9] J. R. Jones, Acta Biomater. **9**, 4457 (2013).
[10] A. Tilocca and A. N. Cormack, J. Phys. Chem. B **111**, 14256 (2007).
[11] M. D. O. Donnell, S. J. J. Watts, R. V. V. Law, R. G. G. Hill, and M. D. O'Donnell, J. Non-Cryst. Solids **354**, 3554 (2008).
[12] F. Fayon, C. Duée, T. Poumeyrol, M. Allix, and D. Massiot, J. Phys. Chem. C **117**, 2283 (2013).
[13] M. Sitarz, K. Bulat, A. Wajda, and M. Szumera, J. Therm. Anal. Calorim. **113**, 1363 (2013).
[14] S. J. Liu, G. Z. Fu, Z. T. Shan, X. R. Ren, Y. F. Zhang, C. F. Zhu, W. He, and Y. Z. Yue, J. Non-Cryst. Solids **383**, 141 (2014).
[15] S. Prabakar, K. J. Rao, and C. N. R. Rao, Mater. Res. Bull. **26**, 285 (1991).
[16] R. J. Kirkpatrick and R. K. Brow, Solid State Nucl. Magn. Reson. **5**, 9 (1995).
[17] M. Nogami, K. Miyamura, Y. Kawasaki, and Y. Abe, J. Non-Cryst. Solids **211**, 208 (1997).
[18] H. Yamashita, H. Yoshino, K. Nagata, H. Inoue, T. Nakajin, and T. Maekawa, J. Non-Cryst. Solids **270**, 48 (2000).
[19] V. G. Plotnichenko, V. O. Sokolov, V. V. Koltashev, and E. M. Dianov, J. Non-Cryst. Solids **306**, 209 (2002).
[20] J. Ide, K. Ozutsumi, H. Kageyama, K. Handa, and N. Umesaki, J. Non-Cryst. Solids **353**, 1966 (2007).
[21] T. Wu, Y. Huang, J. Huang, Y. Huang, P. Zhang, and J. Ma, Appl. Opt. **53**, 4747 (2014).
[22] R. K. Brow, J. Non-Cryst. Solids **263-264**, 1 (2000).
[23] M. G. Mortuza, J. A. Chudek, G. Hunter, and M. R. Ahsan, Chem. Commun. **2000**, 2055.
[24] R. E. Youngman, C. L. Hogue, and B. G. Aitken, MRS Proc. **984**, 0984 (2006).
[25] S. Sakida, T. Nanba, and Y. Miura, Chem. Lett. **35**, 1268 (2006).
[26] J. A. Duffy and D. E. Macphee, J. Phys. Chem. B **111**, 8740 (2007).
[27] W. H. Zachariasen, J. Am. Chem. Soc. **54**, 3841 (1932).
[28] H. Zeng, Q. Jiang, Z. Liu, X. Li, J. Ren, G. Chen, F. Liu, and S. Peng, J. Phys. Chem. B **118**, 5177 (2014).
[29] Q. Jiang, H. Zeng, X. Li, J. Ren, G. Chen, and F. Liu, J. Chem. Phys. **141**, 124506 (2014).
[30] H. Zeng, Q. Jiang, X. Li, F. Ye, T. Tian, H. Zhang, and G. Chen, Appl. Phys. Lett. **106**, 021903 (2015).
[31] P. K. Gupta and J. C. Mauro, J. Chem. Phys. **130**, 094503 (2009).
[32] J. C. Mauro, P. K. Gupta, and R. J. Loucks, J. Chem. Phys. **130**, 234503 (2009).
[33] C. Hermansen, J. C. Mauro, and Y.-Z. Yue, J. Chem. Phys. **140**, 154501 (2014).
[34] C. Hermansen, B. Rodrigues, L. Wondraczek, and Y.-Z. Yue, J. Chem. Phys. **141**, 244502 (2014).
[35] O. V. Mazurin, M. V. Strelsina, and T. P. Shvaiko-Shvaikovskaya, *Handbook of Glass Data: Part C: Ternary Silicate Glasses* (Elsevier, Amsterdam, 1987).
[36] E. M. Rabinovich, M. Ish-Shalom, and A. Kisilev, J. Mater. Sci. **15**, 2027 (1980).

[37]Y.-Z. Yue, J. Non-Cryst. Solids **355**, 737 (2009).
[38]L.-M. Wang, V. Velikov, and C. A. Angell, J. Chem. Phys. **117**, 10184 (2002).
[39]L. M. Martinez and C. A. Angell, Nature **410**, 663 (2001).
[40]C. T. Moynihan, A. J. Easteal, M. A. DeBolt, and J. Tucker, J. Am. Ceram. Soc. **59**, 12 (1976).
[41]D. Miyabe, M. Takahashi, Y. Tokuda, T. Yoko, and T. Uchino, Phys. Rev. B **71**, 172202 (2005).
[42]J. A. Duffy, J. Chem. Educ. **73**, 1138 (1996).
[43]H. Yamashita, H. Yoshino, K. Nagata, I. Yamaguchi, M. Ookawa, and T. Maekawa, J. Ceram. Soc. Jpn. **106**, 539 (1998).
[44]C. Hermansen, R. E. Youngman, J. Wang, and Y.-Z. Yue, J. Chem. Phys. **142**, 184503 (2015).
[45]J. R. Van Wazer, *Phosphorous and Its Compounds* (Interscience, New York, 1958).
[46]J. J. Hudgens, R. K. Brow, D. R. Tallant, and S. W. Martin, J. Non-Cryst. Solids **223**, 21 (1998).
[47]B. Mysen, Am. Mineral. **81**, 1531 (1996).
[48]P. McMillan, Am. Mineral. **69**, 622 (1984).
[49]J. C. Phillips, J. Non-Cryst. Solids **34**, 153 (1979).
[50]J. C. Phillips, J. Non-Cryst. Solids **43**, 37 (1981).
[51]J. C. Phillips, J. Non-Cryst. Solids **44**, 17 (1981).
[52]M. F. Thorpe, J. Non-Cryst. Solids **57**, 355 (1983).
[53]J. C. Phillips and M. F. Thorpe, Solid State Commun. **53**, 699 (1985).
[54]H. He and M. F. Thorpe, Phys. Rev. Lett. **54**, 2107 (1985).
[55]M. F. Thorpe, J. Non-Cryst. Solids **76**, 109 (1985).
[56]M. F. Thorpe and Y. Cai, Phys. Rev. B **40**, 10535 (1989).
[57]M. F. Thorpe, M. V. Chubynsky, D. J. Jacobs, and J. C. Phillips, Glass Phys. Chem. **27**, 160 (2001).
[58]M. M. Smedskjaer, J. C. Mauro, and Y.-Z. Yue, Phys. Rev. Lett. **105**, 115503 (2010).
[59]M. M. Smedskjaer, Front. Mater. **1**, 1 (2014).
[60]B. P. Rodrigues and L. Wondraczek, J. Chem. Phys. **140**, 214501 (2014).
[61]O. V. Mazurin, M. V. Streltsina, and T. P. Shvaiko-Shvaikovskaya, *Handbook of Glass Data* (Elsevier, Amsterdam, 1987).
[62]G. Adam and J. H. Gibbs, J. Chem. Phys. **43**, 139 (1965).
[63]Y. Bottinga and P. Richet, Chem. Geol. **128**, 129 (1996).
[64]G. G. Naumis, Phys. Rev. E **71**, 026114 (2005).
[65]C. A. Angell, Science **267**, 1924 (1995).
[66]O. Laurent, B. Mantisi, and M. Micoulaut, J. Phys. Chem. B **118**, 12750 (2014).
[67]S. W. Martin and C. A. Angell, J. Phys. Chem. **90**, 6736 (1986).
[68]J. C. Mauro, Y.-Z. Yue, A. J. Ellison, P. K. Gupta, and D. C. Allan, Proc. Natl. Acad. Sci. U. S. A. **106**, 19780 (2009).
[69]Q. Zheng, J. C. Mauro, M. M. Smedskjaer, R. E. Youngman, M. Potuzak, and Y.-Z. Yue, J. Non-Cryst. Solids **358**, 658 (2012).